Asian Journal of Chemistry; Vol. 34, No. 11 (2022), 2854-2864

ASIAN JOURNAL OF CHEMISTRY

https://doi.org/10.14233/ajchem.2022.23944

Preparation and Characteristics of Starch Nanocrystals as Corrosion Inhibitor: Experimental and Theoretical Studies

AHMED NEAMAH THAMER[1,2], LEKAA HUSSAIN KADHAM[2] and ISMAEEL M. ALWAAN[3,*]

[1]The General Directorate of Educational in Najaf Al-Ashraf, Iraq
[2]Department of Chemistry, Collage of Education for Girls, University of Kufa, Najaf, Iraq
[3]Department of Chemical Engineering, College of Engineering, University of Kufa, Najaf, Iraq

*Corresponding author: E-mail: ismael.alsallami@uokufa.edu.iq

Received: 1 June 2022; *Accepted*: 9 July 2022; *Published online*: 19 October 2022; AJC-20997

Technological advances have led to sophisticated computer software and programs, along with mathematical and experimental techniques, to envisage corrosion inhibition. Using potentiodynamic polarization measurements, weight loss techniques and quantum chemical calculations, the corrosion inhibition of mild steel was explored in 1 M HCl by employing novel inhibitor starch nanocrystals (SNCs). The structures of starch and its nanocrystals were investigated by FESEM, FTIR, AFM and TEM techniques. In presence of 0.5 g/L SNCs at 293 K, the maximum inhibition efficiency (%IE) was 67%. The results showed that the novel SNC inhibitor follows the Temkin adsorption isotherm. The activation energy, Gibbs free energy, enthalpy and entropy of adsorption were calculated. Quantum chemical calculations further helped to understand the SNC inhibition mechanism through density functional theory (DFT) to estimate possible active centres that could be responsible for SNC adsorption on the surface of mild steel. Moreover, quantum chemical descriptors were computed. The findings indicated that SNCs show a high efficiency for corrosion inhibition.

Keywords: Starch nanocrystals, Corrosion inhibition, Mild steel, Hydrochloric acid, Density functional theory.

INTRODUCTION

Corrosion is a natural phenomenon in which a material is destructed or decays through a destructive attack of a substance through a chemical reaction with its environment [1]. Corrosion is a global problem due to safety loss and economic damage. The losses resulting from corrosion are categorized into indirect and direct losses and the indirect one includes economic losses resulting from efficiency reduction, plant shutdowns, expensive maintenance and product contamination, which can ultimately lead to over-design. Direct losses involve fixing damaged machinery, the cost of replacing corroded structures and substitution of some components [2]. Thus, iron corrosion presents practical and theoretical concerns and has received considerable interest.

Hydrochloric acid (HCl) is widely used for cleaning, pickling, descaling of steel and iron because it is easier to use and more economical than other mineral acids. The HCl is preferred over other acids for pickling and cleaning due to its ability to produce metal chlorides, which are more soluble in an aqueous medium than metal phosphate, sulphates and nitrates [3-5]. The use of corrosion inhibitors is the most effective to protect many alloys and metals against aggressive environments such as alkaline, acidic and saline [5]. By modifying the temperature, removing constituents that facilitate corrosion, removing dissolved O_2 or solid particles, dehumidifying the air and controlling the pH or adding corrosion inhibitors, a less aggressive environment can be obtained [2].

However, the use of traditional corrosion inhibitors, in particular few inorganic substances, including nitrites, chromates and phosphates, is restricted due to their potential environmental risks and toxicity [6-9]. Thus, the establishment of environmentally friendly corrosion inhibitors that used a natural plant extract has attracted substantial attention [10]. Furthermore, in acidic media, organic compounds comprising polar functional groups, such as oxygen, nitrogen and sulphur, in conjugated systems are effective inhibitors of mild steel corrosion [8,11]. Inhibition occurs by producing a surface complex of donor-

acceptor between the *p*- or free electrons of inhibitors and the vacant *d*-orbital of metal atoms [12].

Studies have reported that many nanopolymers, such as glycogen nanoparticles, can be employed in corrosion inhibition [13]. The starch silver nanoparticles were employed to inhibit mild steel corrosion by using the weight loss technique [14,15]. As industrially useful corrosion inhibitors, polymer nanocomposites are recently developed [16]. An environmentally benign corrosion inhibitor that was based on cellulose niacin nanocomposite was utilized to investigate copper corrosion in a NaCl solution [17]. New nanocomposites of copper and nickel oxide nanoparticles embedded in melamine frameworks comprising cellulose nanocrystals were employed to study corrosion [18].

A quantum chemical calculation is a powerful tool to study the mechanisms of corrosion inhibition by using properties, including the energy of lowest unoccupied molecular orbital (E_{LUMO}), energy of highest occupied molecular orbital (E_{HOMO}), global chemical descriptors *e.g*. hardness, softness, chemical potential, electronegativity and electrophilicity. Quantum chemical methods are used for study the behaviour and structure of corrosion inhibitors and to obtain information about the inhibition phenomenon [19,20]. The quantum chemical analysis was employed to determine relationship between the inhibition efficiency molecular and structure of inhibitor compounds and to theoretically investigate molecular and electronic structures of starch nanocrystals (SNCs).

In this study, for mild steel in 1 M HCl, SNCs were used as corrosion inhibitors. Starch nanocrystals exhibit properties that render them green corrosion inhibitors for various metals in aggressive media, such as acidic medium. These compounds have numerous pharmaceutical, medicinal applications *etc*. [21-23]. However, no applications are found for them in corrosion inhibition. Thus, this study assessed the corrosion inhibitory properties of SNCs. For mild steel in 1 M HCl, weight loss measurements were used to study corrosion inhibition by using SNCs as novel corrosion inhibitors. Additionally, the effect of temperature and concentration on the corrosion behaviour was explored in the presence and absence of inhibitors. Moreover, theoretical studies were conducted using DFT for validating the experimental results. To our best of knowledge, no systematic investigation has been performed on the effects of SNCs on the corrosion of mild steel.

EXPERIMENTAL

Iranian mild steel (ST37-2) was obtained from the commercial markets. The corn starch was obtained from Meptico-Lebanon, while the HCl acid (35-38%) with density (1.18 g/mL), *m.w.* (36,46 g/mol) was obtained from S.D. Fine-Chem Ltd., India and sulphuric acid (96%) with density of 1.84 g/mL, *m.w.* of 98.08 g/mol was obtained from Chem-Lab NV Industries zone, Belgium. The stock solution of HCl at the concentration of 1M was prepared by dilution of 37% weight of concentrated HCl using double distilled water.

Preparation of mild steel samples for weight loss method: The metal specimens (ST37-2) were prepared by cutting by laser with a specific dimensions of 2.0 cm × 2.0 cm × 0.18 cm. These pieces were used with further polishing for the exposed flat surface with different grade emery papers (in the range of 180-1200). The specimens were cleaned from grease using double distilled water, absolute ethanol and then finally dried by using acetone. The specimens were kept in the desiccators to avoid the humidity effect until they were utilized corrosion studies. The chemical composition of steel alloy is shown in Table-1.

Preparation of mild steel samples: The material used in the constructing the working electrode was pre-prepared samples of mild steel (ST37-2) having the same dimensions of (2.0 cm × 2.0 cm × 0.18 cm). The specimens were first prepared such that the processed area is the only exposed region that will remain during the test by scraping the steel samples manually, with further burnish for surface with different grade emery papers. The specimens were cleaned from grease using distilled water and absolute ethanol and finally dried by using acetone.

To prepare the samples, the multi-meter wire, one sample, glue, epoxy resin (LOCTITE E-40FL) as insulating material, where the wire was attached to the test sample using glue and left for 1 h to ensure drying time. Thereafter, the epoxy resin was applied on the glued area as well as on the side surfaces of the sample and left for 24 h at room temperature to ensure drying except for the processed region that will remain exposed during the test.

Preparation of SNCs inhibitor: Depending on the botanical source of starch and isolation procedures used, the corn starch nanocrystals were synthesized by acid hydrolysis in accordance with the method followed by Angellier *et al*. [24]. Starch nanocrystals (SNCs) were generally prepared by treating starch suspension with dilute sulphuric acid, where 150 g of starch powders were mixed in 1 L of H_2SO_4 solution and placed at the ambient temperature (293-323 K) for 7 days under continuous stirring (200 rad/min) using the magnetic stirrer. The suspension was separated by Büchner funnel and washed many times with distilled water to remove the acid residuals until the pH becomes netural, and finally the suspension was poured in a glass container and dried the product in oven at 323 K for 72 h.

Characterization: The chemical structure of the starch and starch nanocrystals (SNCs) was investigated using Fourier transform infrared spectroscopy (Alpha-Bruker Co., Germany) at the range of 4000-400 cm^{-1}. The morphology of starch nanocrystals (SNCs) was investigated using field emission scanning electron microscopy (TESCAN MIRA-3 FE-SEM, France) at an acceleration voltage of 1-30 kV. The specimen was sputter-coated with gold (S150A sputter coater) to avoid charging.

TABLE-1
MILD STEEL ALLOY COMPONENTS (wt.%)

Element	C	Si	Mn	P	S	Cr	Mo	Ni	Cu	Al	Fe
Wt%	0.0664	0.0042	0.367	0.0097	0.0077	0.0063	< 0.002	0.0325	0.0049	0.0408	BaL

Transmission electron microscopy (TEM Carl Zeiss-EM10C, Germany) at an acceleration voltage of 100 kV was used to investigate the particle size of modified starch (starch nanocrystals). In addition, atomic force microscopy (AFM) measurements was used to determine the size of starch nanocrystals which was performed on a Multimodal AFM (TT-2 AFM scanning probe microscope, USA).

Weight loss method: Weight loss measurements were performed in 1 M of HCl solution at different temperatures and concentrations by immersing mild steel test coupons in absence and in the presence of the inhibitor. The coupons dimensions of 2.0 cm × 2.0 cm × 0.18 cm were cleaned, weighed and placed in the middle of the corrosive media containing 100 mL of 1 M HCl with and without different concentrations of inhibitor. Then, the samples were placed in a vibrator water bath at a different temperature for certain time periods.

When the treatment time was completed, the test compounds were removed from the electrolyte. Then, these compounds were scrubbed using a soft bristle brush in distilled water to eliminate the corrosion output, dried and weighed. Experiments were conducted in triplicate for each inhibitor concentration, and the average of weight losses was used to calculate the inhibition efficiency and corrosion rate of inhibitors. The variation between initial and specific-period sample weight was used as the weight loss. The weights were estimated using a Sartorius Entris TE64 electronic balance (Germany) having a sensibility of ±0.0001 g. The inhibition efficiency (IE%), corrosion rate (CR) and surface coverage (θ) were determined using the following equations:

$$CR\ (mg\ \ cm^{-2}\ \ h^{-1})r = \frac{\Delta W}{A \cdot t} \quad (1)$$

where ΔW is the weight loss (mg), while A is the area of an exposed surface of the sample (cm^2) and t represents the exposure time (h).

The percentage and efficiency of inhibition (IE %) was calculated according to eqn. 2 [25]:

$$IE\ (\%) = \frac{W_o - W_i}{W_o} \times 100 \quad (2)$$

where W_o = weight loss value in the absence of inhibitor and W_i = weight loss value in the presence of inhibitor.

Evaluation of surface coverage (θ): The surface coverage was determined using eqn. 3 [26]:

$$\text{Surface coverage } (\theta) = \frac{W_o - W_i}{W_o} \quad (3)$$

where W_o and W_i are the weight reduction per unit time with absence and presence of restraint, respectively. Adsorption isotherms are often shown to demonstrate the performance of organic adsorbent type inhibitors. According to this, the relationship between θ and log C was examined to determine whether or not the inhibitor adsorption followed Langmuir, Temkin, Frumkin, Flory-Huggins and Freundlich isotherms [27] by obtaining a linear relationship.

Electrochemical measurements: In a conventional three-electrode cell containing 100 mL of electrolyte at 323 K, electrochemical polarization measurements were performed on an Instrument DY2300 Digi-Ivy potentiostat (USA) having beta software. A saturated calomel electrode (SCE), platinum auxiliary electrode, mild steel specimen were used as the reference electrode, counter electrode (CE) and working electrode (WE), respectively. The current between WE and SCE was measured, and the potential between the reference electrode and WE was measured. Before the experiment, the prepared sample was examined using a multimeter. In the corrosion testing cell, WE was immersed in an acidic medium of 1 M HCl in absence and presence of the inhibitor for 2.5 h before the test at a specific temperature. The open circuit potential (OCP) was measured for 120 s by using this set-up. Linear sweep voltammetry was studied at OCP to reach the steady state. Using an Autolab data acquisition system, polarization curves were plotted. The I_{corr}, CR, and E_{corr} were determined using Tafel extrapolation. For Tafel plots, potentiodynamic polarization curves (current *vs.* potential) were acquired against OCP at a scan rate of 1 mV/s at the potential of –250 to 250 mV. All potentials were determined against SCE. The percentage inhibition efficiency (IE%) was computed using eqn. 4:

$$IE\ (\%) = \frac{i^o_{corr} - i_{corr}}{i^o_{corr}} \times 100 \quad (4)$$

where i^o_{corr} and i_{corr} are the values of corrosion current density in absence and presence of the inhibitors, respectively.

Quantum chemical study: Quantum chemical calculations were performed using the semi-empirical AM1 method to investigate the effect of SNC molecular structure on the inhibition efficiency. All the calculations were conducted by employing complete geometry optimization through DFT by using the B3LYP functional with 6-311++G(d,p) basis set, as implemented in Gaussian 09W program. Frontier molecular orbital energies (E_{LUMO} and E_{HOMO}) are critical for predicting the reactivity of chemical species. The E_{HOMO} is usually associated with a molecule's electron-donating ability. With the increase in E_{HOMO} values, the inhibition efficiency increases. A high E_{HOMO} value indicates that the molecule tends to donate electrons to an appropriate acceptor molecule having a low-energy empty molecular orbital. Low E_{LUMO} values suggest that molecules easily accept electrons from donor molecules [28,29]. Smaller of ΔE_{gap} and larger of dipole moment lead to inhibition efficiency enhancement [30,31]. Quantum chemical descriptors, including E_{LUMO}, E_{HOMO}, energy gap ($\Delta E = E_{LUMO} - E_{HOMO}$), softness, chemical hardness, chemical potential, dipole moment, electronegativity, nucleophilicity, electrophilicity, and number of electrons transferred (ΔN) were calculated.

RESULTS AND DISCUSSION

Characterization of starch nanocrystals (SNCs)

FTIR studies: Fig. 1 shows the chemical structures and nanocrystals of corn starch. The FTIR spectra show a sharp peak in 3000-2800 cm^{-1}, a broad band in 3600-3000 cm^{-1} and a peak in 1200-900 cm^{-1}. These peaks correspond to (C-H) stretching, (O-H) stretching and (C-O-C) stretching vibrations, respectively [32,33]. The absorption peaks seen near 990 and

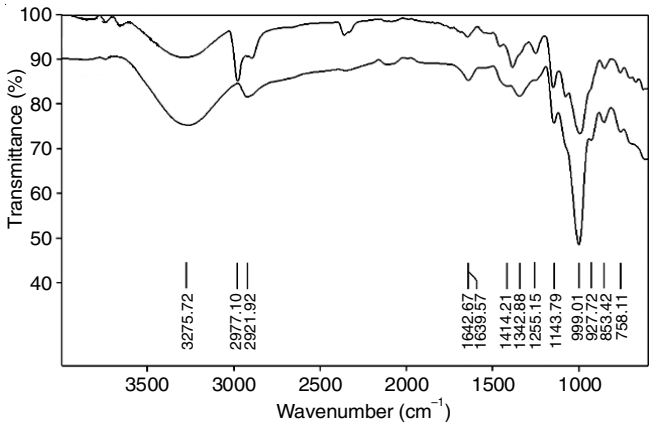

Fig. 1. FTIR spectra of native starch and starch nanocrystals

1150 cm^{-1} correspond to the stretching vibrations of (C-O) [34]. The absorption peak appearing at 1075 cm^{-1} can be assigned to the O-C stretching vibrations for the (C-O-C) group in the glucose ring [35]. Absorption bands seen at 1370 and 1465 cm^{-1} correspond to the in plane bending vibration of O-H of the glucose unit [36]. For these bands, the transmittance intensity was higher in SNCs than in their native counterparts. Similar findings are reported for potato SNCs [37]. The FTIR results of SNC revealed slight changes in the FTIR spectra acquired after and before acid hydrolysis, which indicates that the glucose structure was stable during acid hydrolysis. Similar results are reported by Chen *et al*. [38]. Furthermore, the peak seen at 2924 cm^{-1} for C-H varies with the ratio of amylopectin to amylose [37,39]. A decrease in the amylose ratio leads to an increase in the peak intensity for the (C-H) region. The high C-H peak intensity for corn SNCs proves the selective hydrolysis of amorphous regions, which comprise amylose. The broadening of (O-H) stretching vibration peaks is ascribed to the variation in the intra- and intermolecular hydrogen bonding of starch molecules caused by hydrolysis [40]. The band seen at 1642 cm^{-1} and varies with crystallinity results from water adsorbed (H-O-H) in the amorphous regions of starch [32,41].

SEM studies: The morphology of the starch nanocrystals are shown in Fig. 2. The sample was prepared by coating with a very thin layer of a suitable metal coating (gold) [42]. The corn starch nanocrystals viewed under SEM appeared as square like platelets depending on their crystalline type, while square-like platelets were reported for A-type corn starches [43]. The nanocrystals sizes of starch was in the range of 74-100 nm. The particles seem to have a uniform distribution although some clustering/aggregations were observed.

TEM studies: The morphology and average size of SNCs were explored through transmission electron microscopy (TEM) (Fig. 3). The morphology of insoluble residues after the 7-day hydrolysis of native corn starch granules is shown in Fig. 3. The square platelets can be vaguely seen in the insoluble residues of native starch granules after hydrolysis may be due to different plant sources of starch as well as the aggregation of SNC during monitoring [44]. The size of the residues determined through TEM was 29-66 nm. Few aggregates of >100 nm were found. Similar results are reported by Duan *et al.* [45]. However, different sizes and shapes of SNCs are reported.

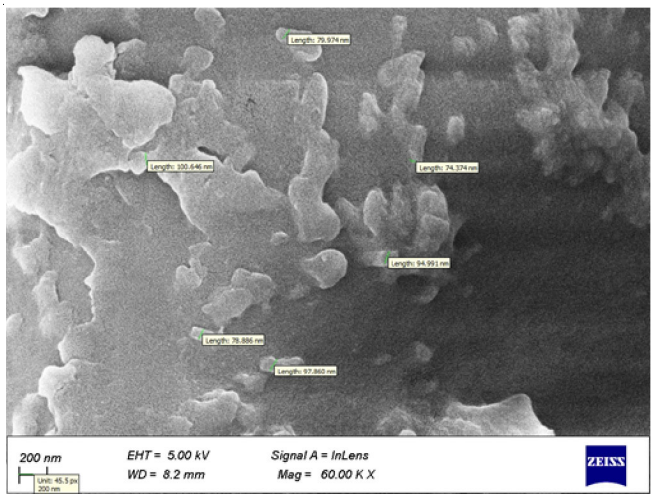

Fig. 2. Scanning electron micrographs of corn starch nanocrystals after curing in 3.16 M H_2SO_4 hydrolysis for 7 days

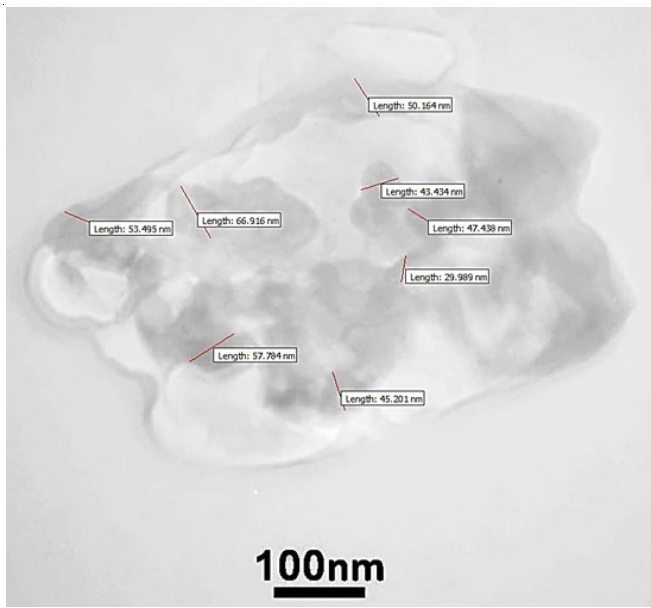

Fig. 3. Transmission electron microscopy of corn starch nanocrystals at curing of 3.16 M H_2SO_4 hydrolysis for 7 days

AFM studies: Atomic force microscopy (AFM) was used to determine the SNC size and its results are shown in Fig. 4a-b. A test was conducted on a mica substrate by preci-pitating a drop of SNC suspension and by drying it at 40 ºC for 20 min. The SNCs showed square platelets irrespective of their botanical origin (Fig. 4a). This finding is in agreement with the literature available on the shape of SNCs [46]. The particle size was evaluated using image analysis software (Nova) acquired with the AFM instrument. The AFM results revealed that the largest size of SNC (65%) was 15 nm (Fig. 4b).

Measurements of weight loss: The corrosion of mild steel in 1M HCl with and without SNCs as inhibitor of corrosion was studied using the weight loss technique over a temperature range of 293-323 k. Fig. 5 illustrates the relationship of metal weight loss *versus* time (h) in 1M HCl without and with an inhibitor (0.2, 0.3, and 0.5 g/L) at 293 K, 303 K, 313 K and 323 K. The weight loss of mild steel with presence of the inhi-

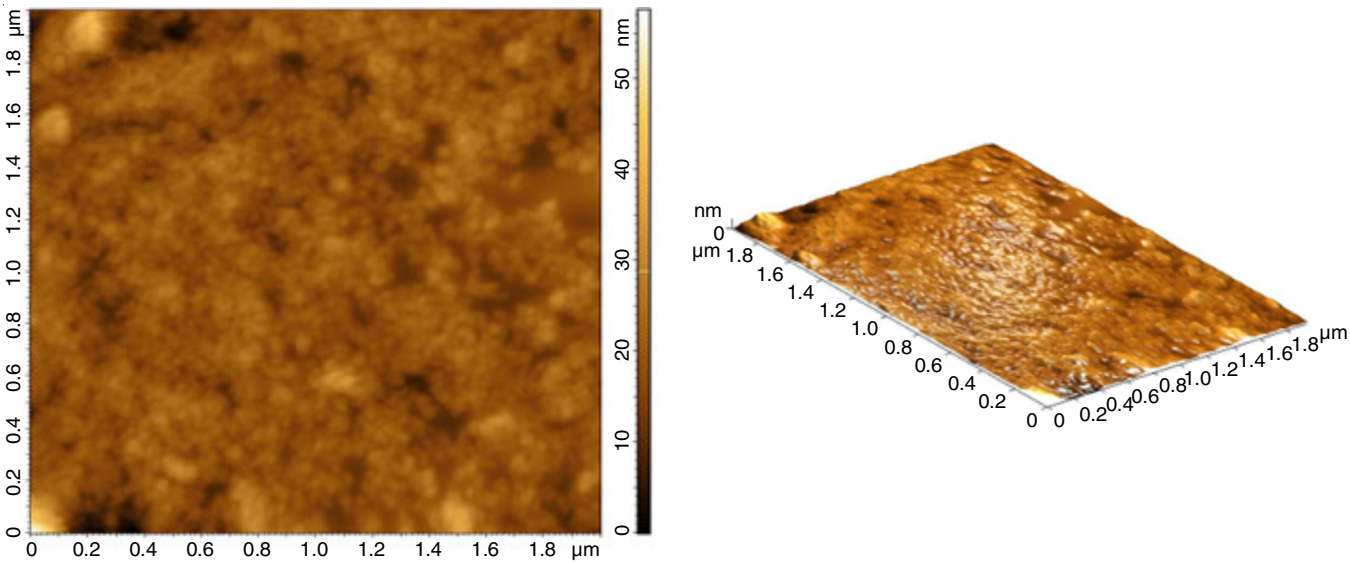

Fig. 4a. Atomic force electron micrographs of corn starch nanocrystals at curing of 3.16 M H_2SO_4 hydrolysis for 7 days

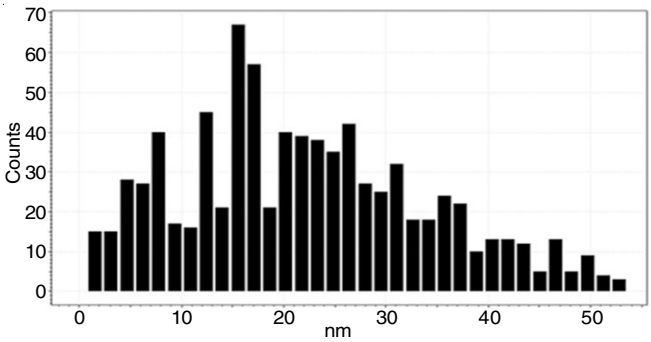

Fig. 4b. Average size range (nm) by AFM of corn starch nanocrystals at curing of 3.16 M H_2SO_4 hydrolysis for 7 days

bitor in the HCl solution was reduced as contrasted to inhibit free solution. The inhibition efficiency and corrosion rates were calculated at the different concentrations of inhibitors and at different temperatures. The results showed that the corrosion rate (CR) was reduced in the presence of the SNCs inhibitor as compared to the situation of absence of loading of the SNCs inhibitor in solution (Table-2). In addition, the corrosion rate increases with temperature increase, indicating that the temperature is a significant operator in the corrosion process [47]. In addition, maximum inhibitor efficiency was 67% at concentration of 0.5 g/L of inhibitor and at 323 K, while the minimum value was 30.6% at inhibitor concentration of 0.2 g/L and at 293 K.

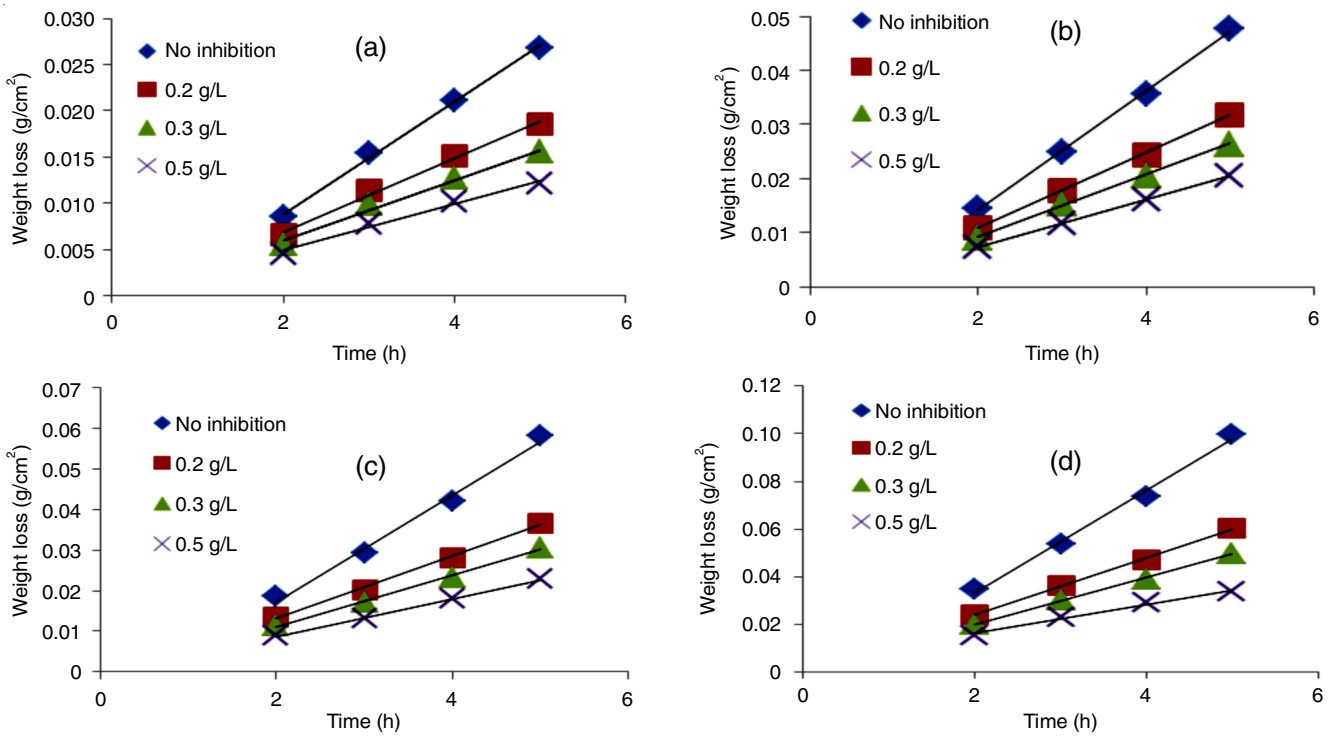

Fig. 5. Weight loss of mild steel against time (h) in 1 M HCl with and without of SNCs blend at (a) 293 K, (b) 303 K, (c) 313 K and (d) 323 K

TABLE-2
CORROSION RATE (CR), INHIBITION EFFICIENCY (IE%) AND SURFACE COVERAGE (θ) OF MILD STEEL IN 1 M HCl FOR DIFFERENT INHIBITOR CONCENTRATIONS AT DIFFERENT TEMPERATURE

Conc. (g/L)	C_R (mg cm^{-2} h^{-1})				Efficiency of inhibitor (IE%)				Degree of surface coverage (θ)			
	293 K	303 K	313 K	323 K	293 K	303 K	313 K	323 K	293 K	303 K	313 K	323 K
Blank	0.670	1.190	1.455	2.490	–	–	–	–	–	–	–	–
0.2	0.465	0.790	0.915	1.455	30.6	33.6	37.1	41.6	0.306	0.336	0.371	0.416
0. 3	0.387	0.650	0.735	1.170	42.3	45.3	49.4	53.0	0.423	0.453	0.494	0.53
0.5	0.302	0.500	0.550	0.820	54.8	58.0	61.8	67.0	0.548	0.618	0.618	0.67

The adsorption of SNCs on the surfaces of mild steel leads to covering of the mild steel surfaces, which leads to the suppression of corrosion of the mild steel and leads to decrease the corrosion rate. The SNCs has a complicated structure (complex polysaccharide), and the FTIR study showed that SNCs contains hydroxyl groups that tend to adsorb on the face of metal surfaces through the electronic pair on the oxygen atoms. These polar groups help in the absorption of SNCs on the surface of mild steel, which prevent the corrosion operation from occurring. It can be suggested that the SNCs can prevent mild-steel corrosion by forming a donor-acceptor surface complex between the free or π-electrons of the inhibitor and vacant *d*-orbital of metal atoms.

Adsorption isotherm: The adsorption isotherm presents the relationship between the surface coverage degree at constant temperature and corrosion inhibition efficiency for different inhibitor concentrations. It provides the information of the nature of interactions between the inhibitor molecular constituents and mild steel surface [48]. Corrosion inhibitor molecules' adsorption occurs on the surface of mild steel through the displacement of water molecule adsorbed onto a metal surface. Moreover, adsorption is dependent on the electronic characteristics, chemical composition, and inhibitor concentration, the nature of metal surface, steric effects, temperature and electrochemical potential at a metal-solution interface and varying degrees of surface-site activity [49]. Fig. 6 shows the results of the relation between the inhibition efficiency (IE%) at different temperatures and inhibitor concentration (C) of SNCs.

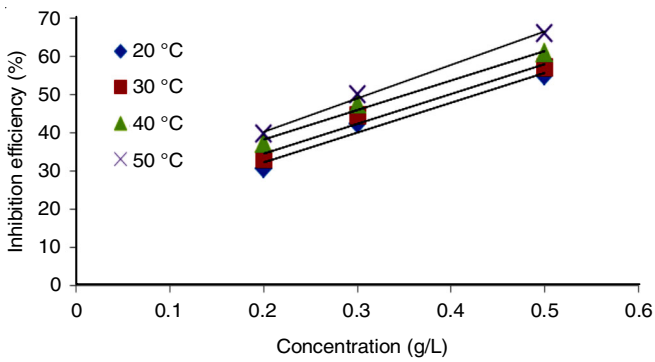

Fig. 6. Inhibition efficiency (IE%) of SNCs *vs.* inhibitor concentration at different temperatures

Several isotherms, such as Freundlich, Langmuir and Temkin, were proposed, which can be used to establish the most appropriate isotherms for experimental data. Adsorption isotherms were used to comprehend interactions between the mild steel surface and inhibitor [50]. In this study, for various inhibitor concentrations in acidic media, the degree of surface coverage values (θ) was evaluated using the weight loss and the changes in θ. Thus, the changes in inhibitor efficiency were determined using the model of Temkin adsorption isotherm. The suppression efficiency increases with the increase in both temperature and restraint concentration rises, *i.e.* with increasing temperature and inhibitor concentration, the inhibition efficacy increases, indicating that the adsorption operation follows the chemical adsorption mechanism [51].

The surface coverage (θ) values justified the behaviour of adsorption of SNCs. The following equation can be used to estimate the surface coverage:

$$\theta = \frac{IE\ (\%)}{100} \quad (5)$$

The surface coverage (θ) values of the inhibitor were used to demonstrate the optimal isotherm for determining adsorption behaviour.

As a good corrosion inhibitor in HCl acid environments, the efficacy of SNCs depends mainly on its ability to adsorb on the metal surface, which is important to explain the interaction mechanism of SNC with mild steel in corrosive media. The optimum isotherm model can be estimated using the correlation coefficient (R^2) [52]. The Temkin isotherm exhibited the optimum correlation coefficient (R^2) value, and thus, is the most satisfactory to represent the experimental data. The (θ) was determined using the Temkin adsorption isotherms. Temkin adsorption isotherm [53,54] is represented as follows:

$$\text{Exp}\ (-2a\theta) = KC \quad (6)$$

where a is the heterogeneous factor of the metal surface that describes the molecular interactions in the adsorption layer and is referred to as the lateral interaction parameter, and K is the adsorption process equilibrium constant.

It is also observed that the empirical information follows the Temkin adsorption isotherm by the linear relevance between the surface coverage and the SNCs inhibitor concentration at all temperature ranges (Fig. 7). Table-3 shows the adsorption variables of Temkin adsorption isotherms of mild steel corrosion in HCl (1M) in the presence of SNCs at 293, 303, 313 and 323 K.

The positive and negative signs of molecular interaction parameters were used to determine the repulsion and attraction forces among adsorbed molecules, respectively. Repulsion occurred between adsorbed molecules because the "A" values are negative (Table-3). The adsorbate and adsorbent intensity is denoted by K. An increase in K values led to more efficient adsorption, which resulted in a better inhibition efficiency. On

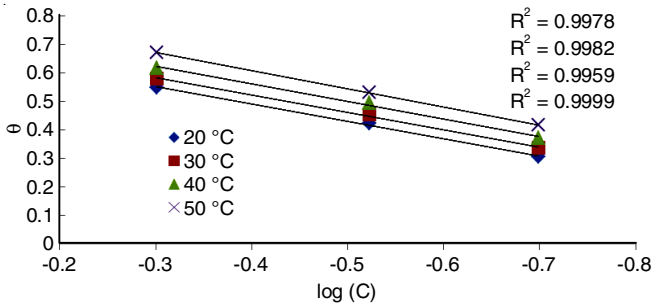

Fig. 7. Surface coverage (θ) *vs.* the log C of SNCs at different temperatures

TABLE-3
TEMKIN ISOTHERM PARAMETERS AT 293, 303, 313 AND 323 K FOR MILD STEEL IN 1 M OF HCl WITH SNCs

Temp. (K)	A	K	R^2
293	-0.825	3.288	0.9978
303	-0.818	3.410	0.9982
313	-0.809	3.544	0.9959
323	-0.784	3.676	0.9999

the metal surface, chemical adsorption may occur due to the increase in the K values with increasing temperature.

Effect of temperature: In 1M HCl at the temperature range of 293-323 K, the effect of temperature on corrosion rate (CR) was studied in the absence and presence of different inhibitor concentrations. The corrosion rate (CR) decreased with the increase in temperature inverse from 293-323 K. The plot of logarithm of CR against different temperatures inverse is shown in Fig. 8 for blank and SNC inhibitors.

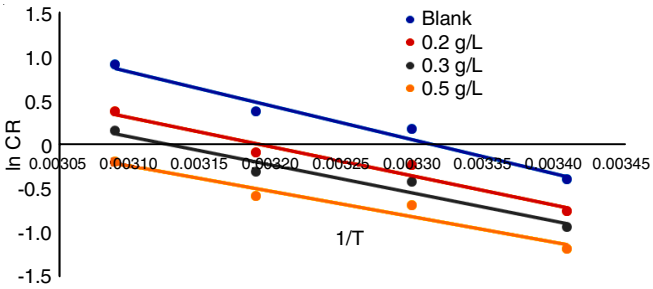

Fig. 8. Logarithm of corrosion rate (CR) against inverse temperature for mild steel with and without SNCs in 1 M of HCl

The straight lines were drawn to show that the relationship between the CR and temperature follows the Arrhenius equation and that the straight-line slope indicates activation energy. The Arrhenius equation can be written as follows [55]:

$$\ln CR = \ln A - \frac{E_a}{RT} \quad (7)$$

From Fig. 8, the slope ($-E_a/R$) of each individual straight line was determined and activation energy (E_a) was calculated by using (E_a = (slope × R) and the calculated value of E_a were summarized in Table-4. It is evident that the apparent activation energy values for the inhibited solutions were lower than that for the non-inhibited one, indicating that the adsorption process is a chemisorption adsorption [56]. It could be attributed to the increase in surface coverage because of the adsorption of the inhibitor molecules on the surface of mild steel as the temperature rises. Next, the adsorption layer blocks the active sites and isolates the mild steel surface from the acidic environment [57]. In this case, the interaction between inhibitor molecules and metal will form coordinate bonds by giving lone electron pairs of oxygen to empty orbitals of iron atoms [58]. This may be explained that the adsorption of SNCs on the metal surface is chemisorption.

TABLE-4
ACTIVATION ENERGY (KJ/mol), ENTHALPY (KJ/mol) AND ENTROPY (J/mol K) OF MILD STEEL CORROSION IN 1 M HCl WITH SNCs INHIBITOR

Conc. (g/L)	E_a (KJ/mol)	ΔH^o_{ads} (KJ/mol)	ΔS^o_{ads} (J/mol K)
Blank	32.090	29.550	-148.665
0.2	27.770	25.157	-164.541
0.3	26.688	24.171	-166.119
0.5	24.082	21.540	-179.580

The values of standard enthalpy of adsorption (ΔH) and the entropy of adsorption (ΔS) for mild steel corrosion in 1M HCl with SNCs inhibitor were calculated using the transition state equation [59]:

$$CR = \frac{RT}{Nh}\exp\left(\frac{\Delta S}{R}\right)\exp\left(-\frac{\Delta H}{RT}\right) \quad (8)$$

Fig. 9 shows a graph between the logarithm of (CR/T) *vs.* inverse temperature (1/T) with the presence and absence of inhibitor. Adsorption enthalpy and adsorption entropy were obtained by slope of ($-\Delta H/R$) and the intersection of the lines, respectively, and the results of various concentrations of inhibitor (0, 0.2, 0.3 and 0.5 g/L) are listed in Table-4. Compared with the blank solution, the positive enthalpy indicates the endothermic nature of mild steel dissolution [60], while, the adsorption enthalpy decreases with inhibitor loading, which proves that the occurance of the chemisorption mechanism [53]. Adsorption entropy has a negative value, without and with inhibitors. A negative ΔS^o value represents an increase in the system order, since adsorption involves an associative mechanism instead of dissociation [53,61]. Adsorption leads to an order by generating an activated complex between the adsorbent and adsorbate, indicating that disorder decreases during the transition from the reactant to activated complex [62]. Moreover, a $-\Delta S^o$ value indicates no significant change in the internal structures of adsorbent during adsorption [63,64].

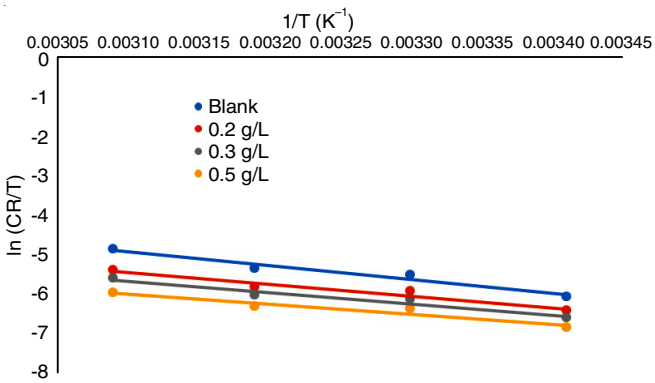

Fig. 9. Transition state plot of the corrosion rate for mild steel in 1 M of HCl with and without SNCs

The interception of a straight line obtained from the log IE% *vs.* log C graph gives the free energy of adsorption (ΔG^{o}_{ads}) (Fig. 10) according to the eqns. 9 and 10 [65]:

$$\log C = \log \frac{\theta}{1-\theta} - \log B \quad (9)$$

where

$$\log B = -1.47 - \left(\frac{\Delta G^{o}_{ads}}{2.303RT} \right) \quad (10)$$

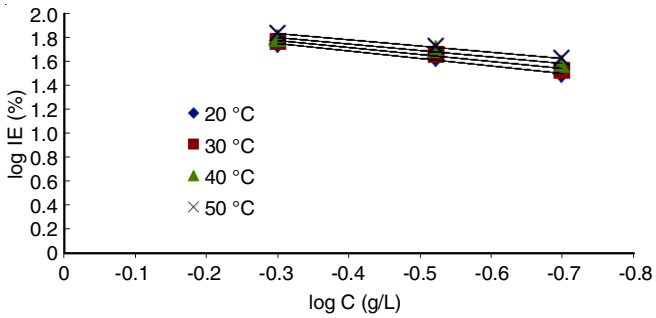

Fig. 10. log IE% *vs.* log C for mild steel corrosion in 1 M HCl for SNCs at 293, 303, 313 and 323 K

Table-5 shows the negative results of free adsorption energy (ΔG^{o}_{ads}) at 293, 303, 313 and 323 K, which indicates that SNCs inhibitor is spontaneously adsorbed.

TABLE-5
GIBBS FREE ENERGY (ΔG^{o}_{ads}) OF MILD STEEL CORROSION IN 1 M OF HCl WITH SNCs

Temp. (K)	ΔG^{o}_{ads} (KJ/mol)
293	-20.628
303	-21.397
313	-22.204
323	-23.041

Potentiodynamic polarization: Fig. 11 shows the potentiodynamic polarization performance for mild steel in an HCl (1M) with 0.5 g/L SNC inhibitor with an immersion time of 2.5 h and at 323 K before test. The immersion time of 2.5 h was used to allow the cathodic and anodic electrodes adequate time for inhibitor adsorption onto the electrode surface to acquire real inhibition data. The potentiodynamic corrosion values acquired from electrochemical studies for mild steel in 1 M HCl acid for SNCs are shown in Table-6. These data can help characterize mild steel (ST-37) sample for corrosion. For the proposed corrosion inhibitor, IE (%) was estimated using eqn. 11 [66]:

$$\text{Inhibition efficiency (IE,\%)} = \frac{i^{o}_{corr} - i_{corr}}{i^{o}_{corr}} \times 100 \quad (11)$$

where i_{corr} and i^{o}_{corr} represent the corrosion current densities with and without the addition of inhibitor, respectively.

In 1 M HCl acid, the use of SNCs as a corrosion inhibitor leads to a decrease in current density and CR at 0.5 g/L concentration. The corrosion current density decreased and the response of inhibition efficiency increased. Inhibitor adsorbed onto the mild steel surface, adsorption is enhanced, while inhibition efficiency improved.

Open circuit potential (OCP): A metal with a lower OCP will dissolve rapidly in the electrolyte compared to a metal with a higher OPC. Thus, it is expected for mild steel to have a poten-tial lower than the OCP based of the corrosion resistance properties of mild steel. The OCP results obtained for all mild steel samples was approximately 0.65 mV.

Mechanism: The efficiency of SNCs to act as a corrosion inhibitor depends on its ability to adsorb on the metal surface. The inhibition efficiency of organic matter is mostly related to its adsorption on the metal surface at constant temperatures [67]. It is well recognized that the adsorption of an restraint always represents a supplanting reaction, which involves the

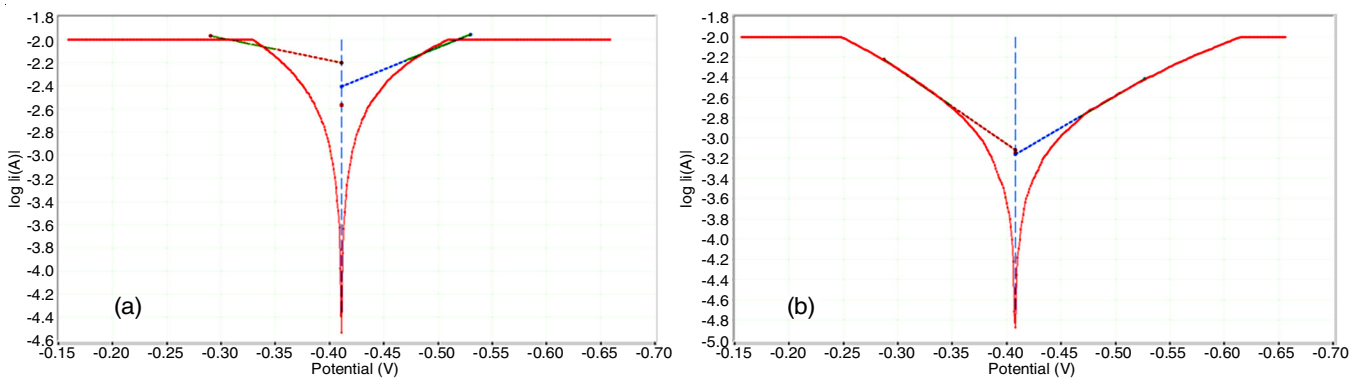

Fig. 11. Potentiodynamic polarization curves of mild steel in 1 M HCl solution measured in the (a) absence and (b) presence 0.5 g/L of SNCs inhibitor after pass 2.5 h of immersion

TABLE-6
ELECTROCHEMICAL PARAMETERS OBTAINED FROM POLARIZATION MEASUREMENT OF MILD STEEL IN 1 M HCl IN THE PRESENCE AND ABSENCE OF 0.5 g/L OF SNCs INHIBITOR AFTER PASS 2.5 h OF IMMERSION

Conc. (g/L)	E_{corr} (mV)	i_{corr} (μA/cm^2)	β_c (mV/dec)	β_a (mV/dec)	R_{CT} (Ω)	Inhibition efficiency (%)
Blank	-0.411	2.732×10^{-3}	3.782	1.940	9.404	–
0.5	-0.408	7.075×10^{-4}	6.252	7.432	36.32	74.1

removal of H_2O molecules to adsorb on the metal roof, where the organic inhibitor molecules replace the H_2O molecules on the metal roof [68] as represented in eqn. 12:

$$Org_{(sol)_1} + nH_2O_{(ads)_1} \longleftrightarrow Org_{(ads)_2} + nH_2O_{(sol)_2} \quad (12)$$

where the organic molecules of $Org_{(sol)_1}$ and $Org_{(ads)_2}$, represent the aqueous solution and the adsorbed solution on the steel roof, respectively. The $H_2O_{(ads)_1}$ represents a H_2O molecule on the steel roof and n represents the number of water molecules replaced by one unit of SNCs [68].

Several parameters control the adsorption of the inhibitor on the metal surface. Physico-chemical properties mainly effect the adsorption of these molecules [69,70], which include the structure of electronic, steric factor, density of electronic at the donor site, functional groups and the size of molecular which has the greatest effect [71]. According to the FTIR studies, the SNCs inhibitor contains oxygen atoms in its structure, therefore carry more pairs of free electrons. As a result, the SNCs inhibitor is expected to adsorb on the metal surface due to the unoccupied *d*-orbitals with electrons of the metal atoms, which leads to covering a large surface area of mild steel. Cathodic restraints reduce least reaction that occurs at the cathode, where the cathodic and anodic reactions correspond to OH^- and Fe^{2+}, respectively [72] as shown in eqns. 13 and 14:

$$Fe \longrightarrow Fe^{2+} + 2e^- \text{ (anodic reaction)} \quad (13)$$

$$2H_2O + O_2 + 4e^- \longrightarrow 4OH^- \text{ (cathodic reaction)} \quad (14)$$

The reaction of anodic inhibition on the metal surface is dominated by a configuration of a complex (Fe^{2+}–SNCs) on the metal surface anodic positions, whereas the cathodic inhibition reaction is controlled by a formation of an insoluble substance on the cathodic sites of the metal complex [72].

Quantum molecular descriptors: Quantum chemical descriptors, including E_{LUMO}, E_{HOMO}, energy gap ($\Delta E = E_{LUMO} - E_{HOMO}$), softness, chemical hardness, electronegativity, dipole moment, chemical potential, electrophilicity, ΔN and nucleophilicity, are useful and effective tools for the corrosion study of metals [73]. Table-7 presents the molecular properties of starch nanocrystals and starch for metal iron corrosion in aqueous solutions. The effect of each descriptor on the inhibition efficiency order for starch and starch nanocrystals is discussed. HOMO, a quantum chemical parameter, is associated with a molecule's electron-donating ability. Thus, with the increasing E_{HOMO} values, the inhibition efficiency increases. A higher value of E_{HOMO} for nano starch (–0.2837 a.u) than for starch (–0.3165 a.u) revealed that nano starch donates electrons to appropriate acceptor molecules (iron) having a low energy empty orbital [73]. This result agrees with the experimental data of weight loss.

The energy gap (ΔE) is a crucial descriptor of the function of reactivity of inhibitor molecules to adsorption on a metal surface. A decrease in ΔE leads to the increase in molecule reactivity. The optimum corrosion inhibitor is obtained when the inhibitor molecule shows a low energy gap. Low ionization energy is required to remove one electron from the last occupied orbital. Additionally, a molecule having a low energy gap is highly polarisable, associated with a low kinetic stability and high chemical activity and is termed as a soft molecule. Inhibitor SNC shows the lowest energy gap (Table-7). The SNC molecule from starch could show high performance as corrosion inhibitor. Similarly, a low electronegativity (X) represents good corrosion inhibition. SNC is a better corrosion inhibitor than starch (Table-7), since SNCs had the lowest electronegativity. Thus, it exhibited high reactivity to show high inhibition efficiency.

The softness (S) and hardness (η) are important to measure the molecular reactivity and stability. Hard molecules have large energy gaps whereas soft molecules have small energy gaps. Thus, for bulk metals in acidic media, molecules with the minimum global hardness are good corrosion inhibitors. By contrast, inhibitor adsorption onto a metal surface occurs at the position of a molecule having the lowest hardness and highest softness; the highest global softness shows the maximum inhibition efficiency. Thus, SNCs have the maximum softness and minimum hardness (Table-7). Therefore, SNCs are the better choice to inhibit mild steel corrosion in acidic media than starch. These finding agrees with the weight loss test results.

Conclusion

In this study, the corrosion inhibition of mild steel in the absence and presence of starch nanocrystals (SNCs) in 1M HCl medium was explored theoretically and experimentally through the potentiodynamic polarization, weight loss and DFT at the temperature range of 293-323 K. The favourable conditions utilized to prepare nanocrystals resulted in a decreased particle size and led to nanocrystals with a size of 30-70 nm. The SNC exhibit a morphology of square platelets. Both SNC and native starch showed an A-type crystalline pattern. Compared with the weight loss of blank solution, that of mild steel decreased with inhibitor loading in the acid solution. The prepared SNCs exhibited high inhibition efficiencies against mild steel corrosion in 1 M HCl. Their inhibition efficiency increased in 1M HCl at 0.5 g/L SNCs and 323 K (5 h) with the increase in the inhibitor concentration and temperature to 67%. The FTIR studies of SNCs and starch showed no significant changes in the starch and SNC structures after and before acid hydrolysis because glucose units had a stable structure. The FTIR spectra showed that the natural polymer structure contains O-H groups, which improved the adhesion of SNCs onto the iron metal surface. Electrochemical measurements and mass loss strongly agreed with each other. The molecular dynamics simulation and quantum chemical calculations based on DFT were used to obtain the possible active centres responsible for SNC's adsorption on the mild steel surface. For SNCs, the corrosion inhibition efficiency increased with the decrease in ΔE_{gap}, compared with

TABLE-7
QUANTUM CHEMICAL PARAMETERS CALCULATED BY DFT LEVEL USING THE B3LYP/6-311G++ (d, p) BASIS SET

Compounds	ΔE_{gap}	E_{HOMO}	E_{LUMO}	DM	Ω	X	S	η	ΔN	ε	ω
Nano starch	0.2894	-0.2837	0.00568	6.0712	0.0668	-0.3196	6.9109	0.1447	0.9606	14.979	0.0667
Starch	0.3134	-0.3164	-0.0031	7.2840	0.1567	-0.1390	0.6383	0.1567	2.0393	3.0664	0.15667

that for starch. The prepared SNCs have low electronegativity, hence, exhibit high reactivity, which leads to a high inhibition efficiency. The SNCs also exhibited the lowest hardness and highest softness; the highest global softness leads to the highest inhibition efficiency (IE%).

CONFLICT OF INTEREST

The authors declare that there is no conflict of interests regarding the publication of this article.

REFERENCES

1. L.C. Murulana, M.M. Kabanda and E.E. Ebenso, *J. Mol. Liq.*, **215**, 763 (2016); https://doi.org/10.1016/j.molliq.2015.12.095
2. J.A. Rodríguez, J. Cruz-Borbolla, P.A. Arizpe-Carreón and E. Gutiérrez, *Materials*, **13**, 5656 (2020); https://doi.org/10.3390/ma13245656
3. A.A. El-Meligi, *Recent Patents on Corros. Sci.*, **2**, 22 (2010).
4. K.C. Emregül and M. Hayvalí, *Corros. Sci.*, **48**, 797 (2006); https://doi.org/10.1016/j.corsci.2005.03.001
5. P. Preethi Kumari, P. Shetty and S.A. Rao, *Arab. J. Chem.*, **10**, 653 (2017); https://doi.org/10.1016/j.arabjc.2014.09.005
6. A.M. Fekry and R.R. Mohamed, *Electrochim. Acta*, **55**, 1933 (2010); https://doi.org/10.1016/j.electacta.2009.11.011
7. G. Gece, *Corros. Sci.*, **53**, 3873 (2011); https://doi.org/10.1016/j.corsci.2011.08.006
8. E.E. Oguzie, *Mater. Lett.*, **59**, 1076 (2005); https://doi.org/10.1016/j.matlet.2004.12.009
9. Y. Li, P. Zhao, Q. Liang and B. Hou, *Appl. Surf. Sci.*, **252**, 1245 (2005); https://doi.org/10.1016/j.apsusc.2005.02.094
10. D. Marunkic, B. Jegdic, J. Pejic, M. Miloševic, A. Marinkovic and B. Radojkovic, *Mater. Corros.*, **73**, 1286 (2022); https://doi.org/10.1002/maco.202213079
11. M. Lebrini, M. Lagrenée, H. Vezin, M. Traisnel and F. Bentiss, *Corros. Sci.*, **49**, 2254 (2007); https://doi.org/10.1016/j.corsci.2006.10.029
12. K.M. Shainy, P.R. Ammal, K.N. Unni, S. Benjamin and A. Joseph, *J. Bio- Tribo-Corrosion*, **2**, 1 (2016); https://doi.org/10.1007/s40735-016-0050-3
13. M. Pais, S.D. George and P. Rao, *Int. J. Biol. Macromol.*, **182**, 2117 (2021); https://doi.org/10.1016/j.ijbiomac.2021.05.185
14. E.D. Paul, A.F. Egbuniwe and P.A. Ekwumemgbor, *ATBU J. Sci. Technol. Educ.*, **6**, 176 (2018).
15. A. Kausar, *J. Plast. Film Sheeting*, **35**, 181 (2019); https://doi.org/10.1177/8756087918806027
16. K. Sharma, M.S. Goyat and P. Vishwakarma, *IOP Conf. Series: Mater. Sci. Eng.*, **983**, 012016 (2020); https://doi.org/10.1088/1757-899X/983/1/012016
17. M.S. Hasanin and S.A. Al Kiey, *Int. J. Biol. Macromol.*, **161**, 345 (2020); https://doi.org/10.1016/j.ijbiomac.2020.06.040
18. H. M. A. El-Lateef and M. Gouda, *J. Mol. Liq.*, **342**, 116960 (2021); https://doi.org/10.1016/j.molliq.2021.116960
19. H. Ju, L. Ding, C. Sun and J.-J. Chen, *Adv. Mater. Sci. Eng.*, **2015**, 519606 (2015); https://doi.org/10.1155/2015/519606
20. G. Gece, *Corros. Sci.*, **50**, 2981 (2008); https://doi.org/10.1016/j.corsci.2008.08.043
21. M.A. Odeniyi, O.A. Omoteso, A.O. Adepoju and K.T. Jaiyeoba, *Polym. Med.*, **48**, 41 (2018); https://doi.org/10.17219/pim/99993
22. A. Caldonazo, S.L. Almeida, A.F. Bonetti, R.E.L. Lazo, M. Mengarda and F.S. Murakami, *Int. J. Biol. Macromol.*, **181**, 697 (2021); https://doi.org/10.1016/j.ijbiomac.2021.03.061
23. M.A.V.T. Garcia, C.F. Garcia and A.A.G. Faraco, *Stärke*, **72**, 1900270 (2020); https://doi.org/10.1002/star.201900270
24. H. Angellier, L. Choisnard, S. Molina-Boisseau, P. Ozil and A. Dufresne, *Biomacromolecules*, **5**, 1545 (2004); https://doi.org/10.1021/bm049914u
25. R. Govindasamy and S. Ayappan, *J. Chil. Chem. Soc.*, **60**, 2786 (2015); https://doi.org/10.4067/S0717-97072015000100004
26. S.K. Shukla, A.K. Singh and M.A. Quraishi, *Int. J. Electrochem. Sci.*, **7**, 3371 (2012).
27. K. Stanly Jacob and G. Parameswaran, *Corros. Sci.*, **52**, 224 (2010); https://doi.org/10.1016/j.corsci.2009.09.007
28. S. Xia, M. Qiu, L. Yu, F. Liu and H. Zhao, *Corros. Sci.*, **50**, 2021 (2008); https://doi.org/10.1016/j.corsci.2008.04.021
29. E.E. Ebenso, T. Arslan, F. Kandemirli, N. Caner and I. Love, *Int. J. Quantum Chem.*, **110**, 1003 (2010); https://doi.org/10.1002/qua.22249
30. D.Q. Zhang, Z.X. An, Q.Y. Pan, L.X. Gao and G.D. Zhou, *Corros. Sci.*, **48**, 1437 (2006); https://doi.org/10.1016/j.corsci.2005.06.007
31. Y.M. Tang, W.Z. Yang, X.S. Yin, Y. Liu, R. Wan and J.T. Wang, *Mater. Chem. Phys.*, **116**, 479 (2009); https://doi.org/10.1016/j.matchemphys.2009.04.018
32. A. Mukurumbira, M. Mariano, A. Dufresne, J.J. Mellem and E.O. Amonsou, *Int. J. Biol. Macromol.*, **102**, 241 (2017); https://doi.org/10.1016/j.ijbiomac.2017.04.030
33. R. Kizil, J. Irudayaraj and K. Seetharaman, *J. Agric. Food Chem.*, **50**, 3912 (2002); https://doi.org/10.1021/jf011652p
34. E.F. Magomedova, V.V. Pinyaskin and A.S. Aminova, *Pharm. Chem. J.*, **41**, 474 (2007); https://doi.org/10.1007/s11094-007-0104-4
35. H. Wang, C. Liu, R. Shen, J. Gao and J. Li, *Polymers*, **13**, 431 (2021); https://doi.org/10.3390/polym13030431
36. K. Zhong, Z.-T. Lin, X.-L. Zheng, G.-B. Jiang, Y.-S. Fang, X.-Y. Mao and Z.-W. Liao, *Carbohydr. Polym.*, **92**, 1367 (2013); https://doi.org/10.1016/j.carbpol.2012.10.030
37. M.J. Jivan, A. Madadlou and M. Yarmand, *Food Chem.*, **141**, 1661 (2013); https://doi.org/10.1016/j.foodchem.2013.04.071
38. L. Chen, Z. Zhang, Z. Zhao, X. Wang and X. Chen, *Carbohydr. Polym.*, **112**, 520 (2014); https://doi.org/10.1016/j.carbpol.2014.06.040
39. S.A. Oyeyinka, S. Singh, P.O. Adebola, A.S. Gerrano and E.O. Amonsou, *Carbohydr. Polym.*, **133**, 171 (2015); https://doi.org/10.1016/j.carbpol.2015.06.100
40. S. Wang, X. Hu, Z. Wang, Q. Bao, B. Zhou, T. Li and S. Li, *Ultrason. Sonochem.*, **64**, 105054 (2020); https://doi.org/10.1016/j.ultsonch.2020.105054
41. F. Luo, Q. Huang, X. Fu, L. Zhang and S. Yu, *Food Chem.*, **115**, 563 (2009); https://doi.org/10.1016/j.foodchem.2008.12.052
42. N. Mazumder, S. Umashankar, B. Ratnakar, K.K. Mahato and F.J. Kao, *Pap.*, **12**, 105 (2017); https://doi.org/10.1364/FIO.2017.FTu4B.4
43. D. LeCorre, J. Bras and A. Dufresne, *J. Nanopart. Res.*, **13**, 7193 (2011); https://doi.org/10.1007/s11051-011-0634-2
44. A.L.I.H. Kamel, *Int. J. Adv. Sci. Eng. Technol.*, **6**, 50 (2018).
45. B. Duan, P. Sun, X. Wang and C. Yang, *Starch/Staerke*, **63**, 528 (2011); https://doi.org/10.1002/star.201000136
46. S.V. Kumar, V.A.S. kumar and S. Kumar, *Stärke*, **151**, 10 (2018); https://doi.org/10.1002/star.201700026
47. S. Feliu, Jr., L. Veleva and F. García-Galvan, *Metals*, **9**, 591 (2019); https://doi.org/10.3390/met9050591
48. E.A. Noor and A.H. Al-Moubaraki, *Mater. Chem. Phys.*, **110**, 145 (2008); https://doi.org/10.1016/j.matchemphys.2008.01.028
49. A.A.S. Begum, R.M.A. Vahith, V. Kotra, M.R. Shaik, A. Abdelgawad, E.M. Awwad and M. Khan, *Coatings*, **11**, 106 (2021); https://doi.org/10.3390/coatings11010106
50. S.A. Xavier Stango and U. Vijayalakshmi, *J. Asian Ceram. Soc.*, **6**, 20 (2018); https://doi.org/10.1080/21870764.2018.1439608
51. N. Zulfareen, K. Kannan, T. Venugopal and S. Gnanavel, *Arab. J. Chem.*, **9**, 121 (2016); https://doi.org/10.1016/j.arabjc.2015.08.023

52. N. Hamid, M.S. Abdul Munaim and M.N. Abu Seman, *Int. J. Eng. Technol. Sci.*, **3**, 44 (2016); https://doi.org/10.15282/ijets.6.2016.1.7.1057
53. I.M. Alwaan and F.K. Mahdi, *Int. J. Chem. Eng.*, **2016**, 5706432 (2016); https://doi.org/10.1155/2016/5706432
54. M. Messali, H. Lgaz, R. Dassanayake, R. Salghi, S. Jodeh, N. Abidi and O. Hamed, *J. Mol. Struct.*, **1145**, 43 (2017); https://doi.org/10.1016/j.molstruc.2017.05.081
55. M. Jeeva, G.V. Prabhu, M.S. Boobalan and C.M. Rajesh, *J. Phys. Chem. C*, **119**, 22025 (2015); https://doi.org/10.1021/acs.jpcc.5b05788
56. I. Dehri and M. Özcan, *Mater. Chem. Phys.*, **98**, 316 (2006); https://doi.org/10.1016/j.matchemphys.2005.09.020
57. I.A. Alkadir Aziz, I.A. Annon, M.H. Abdulkareem, M.M. Hanoon, M.H. Alkaabi, L.M. Shaker, A.A. Alamiery, W.N.R. Wan Isahak and M.S. Takriff, *Lubricants*, **9**, 122 (2021); https://doi.org/10.3390/lubricants9120122
58. D. Quy Huong, T. Duong and P.C. Nam, *ACS Omega*, **4**, 14478 (2019); https://doi.org/10.1021/acsomega.9b01599
59. N.B. Iroha and O. Akaranta, *SN Appl. Sci.*, **2**, 1514 (2020); https://doi.org/10.1007/s42452-020-03296-8
60. M. Yadav, D. Behera, S. Kumar and R.R. Sinha, *Ind. Eng. Chem. Res.*, **52**, 6318 (2013); https://doi.org/10.1021/ie400099q
61. N. Kavitha and P. Manjula, *Int. J. Innov. Res. Sci. Eng. Technol*., **5**, 6761 (2016).
62. V.R. Saliyan and A.V. Adhikari, *Bull. Mater. Sci.*, **31**, 699 (2008); https://doi.org/10.1007/s12034-008-0111-4
63. A.Y. El-Etre, *Corros. Sci.*, **45**, 2485 (2003); https://doi.org/10.1016/S0010-938X(03)00066-0
64. P. Saha and S. Chowdhury, *Thermodynamics*, **16**, 349 (2011); https://doi.org/10.5772/13474
65. S. Bilgiç and M. Sahin, *Mater. Chem. Phys.*, **70**, 290 (2001); https://doi.org/10.1016/S0254-0584(00)00534-4
66. O.S.I. Fayomi, M. Abdulwahab, A.P.I. Popoola and F. Asuke, *J. Mar. Sci. Appl.*, **14**, 459 (2015); https://doi.org/10.1007/s11804-015-1333-7
67. N. Noorollahy Bastam, H.R. Hafizi Atabak, F. Atabaki, M. Radvar and S. Jahangiri, *Iran. J. Chem. Chem. Eng.*, **39**, 113 (2020); https://doi.org/10.30492/ijcce.2020.38997
68. S. Cheng, S. Chen, T. Liu, X. Chang and Y. Yin, *Mater. Lett.*, **61**, 3276 (2007); https://doi.org/10.1016/j.matlet.2006.11.102
69. D.M. Gurudatt, K.N. Mohana and H.C. Tandon, *Mater. Discov.*, **2**, 24 (2015); https://doi.org/10.1016/j.md.2016.03.005
70. M.A. Najafi Lahiji, A.R. Keshtkar and M.A. Moosavian, *Int. J.*, **36**, 340 (2018); https://doi.org/10.1080/02726351.2016.1248262
71. M. Yadav, D. Behera, S. Kumar and P. Yadav, *Chem. Eng. Commun.*, **202**, 303 (2015); https://doi.org/10.1080/00986445.2013.841148
72. H. Hussein, M. Shaffei, N. Khatab, A. Awad, N. Shabaan and M. Shalaby, *Egypt. J. Chem.*, **64**, 5957 (2021); https://doi.org/10.21608/ejchem.2021.88962.4272
73. N. Kazim, *Egypt. J. Chem.*, **64**, 3405 (2021); https://doi.org/10.21608/ejchem.2021.62383.3338